Magic wavelengths of the Ca^+ ion for circularly polarized light

Jun Jiang,* Li Jiang, Xia Wang, Deng-Hong Zhang, Lu-You Xie, and Chen-Zhong Dong
Key Laboratory of Atomic and Molecular Physics and Functional Materials of Gansu Province, College of Physics and Electronic Engineering, Northwest Normal University, Lanzhou 730070, People's Republic of China
(Received 29 March 2017; revised manuscript received 4 August 2017; published 12 October 2017)

The dynamic dipole polarizabilities of low-lying states of Ca^+ ions for circularly polarized light are calculated by using the relativistic configuration interaction plus core polarization approach. The magic wavelengths are determined for the magnetic sublevel transitions $4s_{\frac{1}{2},m} \rightarrow 4p_{j',m'}$ and $4s_{\frac{1}{2},m} \rightarrow 3d_{j',m'}$ with total angular momentum j' and its components m'. In contrast to the case of linearly polarized light, several additional magic wavelengths are found for these transitions. We suggest that accurate measurements on the magic wavelengths near 851 nm for the $4s_{\frac{1}{2},m} \rightarrow 4p_{\frac{3}{2},m'}$ transitions can be used to determine the ratio of the oscillator strengths for the $4p_{\frac{3}{2}} \rightarrow 3d_{\frac{3}{2}}$ and $4p_{\frac{3}{2}} \rightarrow 3d_{\frac{5}{2}}$ transitions.

DOI: 10.1103/PhysRevA.96.042503

I. INTRODUCTION

The magic wavelength is the wavelength of an externally applied laser field at which the ac Stark shift of a particular transition energy of the trapped atoms goes to zero, which was introduced in Refs. [1,2]. This effect is widely used for optical trapping. Since then, the magic wavelength has been extensively utilized in ultraprecise optical lattice clocks [3–9] and state-insensitive quantum engineering [10,11].

The magic wavelengths of alkali-metal and alkaline-earth-metal atoms for linearly polarized light have been studied extensively in both experiment and theory [12–18]. For alkali-metal atoms in a linearly polarized light field, the potential is the same for the two spin states $m_s = \pm\frac{1}{2}$ of the atoms in their respective ground states [19], which means the magnetic sublevels $m_j = \pm\frac{1}{2}$ of the ground states are degenerate. However, in the case of circularly polarized laser light, this degeneracy is lifted. In this case, the laser field acts as a "fictitious magnetic field" due to the vector polarizabilities that are absent for linearly polarized light [20], and the ac Stark shift of the ground states of the atoms behaves like a pure Zeeman shift [21]. Due to this effect, the magic wavelengths for circularly polarized light have significant applications, such as in the magnetic-sublevel selective trapping and far-off-resonance laser trapping [10,19,22]. For this reason, the magic wavelengths of alkali-metal atoms for circularly polarized light have been studied as well [10,23–25].

Precision measurements of magic wavelengths and magic-zero wavelengths (at which the polarizability for a certain atomic state is zero) are also very important in the studies of atomic structure [14]. They can be used to test atomic structure calculations and also provide high-precision determination on the ratio of line strengths or transition matrix elements [26–29]. For example, the ratio of ^{87}Rb D-line dipole matrix elements was determined with an accuracy up to 15 ppm by means of high-precision measurements of the D-line magic-zero wavelength [30]. Moreover, the measurement on the longest magic-zero wavelength of the ground state of potassium determined the ratio of D1 and D2 line strengths with a record precision, i.e., 2.0005(40) [26].

All-optical trapping of ions has been achieved in experiment [31,32] and thus it is very important to pursue the trapping ions at a magic wavelength. As one of the alkali-metal-like ions, the Ca^+ ion is one of the candidates for optical frequency standard and quantum computing [33–37]. Just very recently, two magic wavelengths of the $^{40}Ca^+$ $4s \rightarrow 3d_{\frac{5}{2},m}$ $(m = \frac{1}{2}, \frac{3}{2})$ clock transitions for linearly polarized light have been measured with very high accuracy [14]. The measurement of these two magic wavelengths determines the ratio of the oscillator strengths for the $4s \rightarrow 4p_{\frac{1}{2}}$ and $4s \rightarrow 4p_{\frac{3}{2}}$ transitions with errors less than 0.5%, which is much better than the results obtained from traditional spectroscopic techniques.

In this paper, we calculated the energy levels, electric dipole matrix elements, and static polarizabilities of Ca^+ ions by using the relativistic configuration interaction plus core polarization (RCICP) approach. Moreover, the dynamic dipole polarizabilities of the $4s$, $4p_j$ $(j = \frac{1}{2}, \frac{3}{2})$, and $3d_j$ $(j = \frac{3}{2}, \frac{5}{2})$ states of Ca^+ were calculated for circularly polarized light. The magic wavelengths for each of the existing magnetic sublevel transitions were determined. In the following section, a brief description of the theoretical method is given. In Sec. III, the dynamic polarizabilities and magic wavelengths are discussed. Finally, a few conclusions are made in Sec. IV. The atomic units ($m_e = 1$, $e = 1$, $\hbar = 1$) are used throughout this paper unless stated otherwise, The speed of light is chosen to be $c = 137.0359991$.

II. THEORETICAL METHOD

In the present paper, the energy levels and transition arrays involved are calculated by using the RCICP method which has been developed recently by us [39]. The method is similar to the one used by Tang *et al.* in the calculations of magic wavelengths of Ca^+ for linearly polarized light [15]. The only difference is that they used the B-spline basis to expand atomic state wave functions instead of the L- and S-spinor basis as we used. S-spinors can be treated as relativistic generalizations of the Slater-type orbitals. L-spinors can be treated as relativistic generalizations of the Laguerre-type orbitals [40,41]. The Laguerre bases are orthogonal to each other and can be enlarged towards completeness without the problem of linear dependence, which guarantees tiny errors

*phyjiang@yeah.net

TABLE I. Magic wavelengths (in nm) for the $4s_{\frac{1}{2},m} \rightarrow 4p_{\frac{1}{2},m'}$ transitions of Ca^+ for left-handed circularly polarized light, which are compared with the ones for linearly polarized light. $\Delta\lambda$ (in nm) denotes the difference of magic wavelengths between the two kinds of polarization. λ_{res} represents the wavelength of resonance transition. The numbers in the parentheses are uncertainties caused by assuming that matrix elements are calculated within ±2% uncertainties.

Resonances	λ_{res}	$\mathcal{A}=0$	$\mathcal{A}=-1$					
		λ_{magic}	λ_{magic}	$\Delta\lambda$	λ_{magic}	$\Delta\lambda$	λ_{magic}	$\Delta\lambda$	λ_{magic}	$\Delta\lambda$
		$4s_{\frac{1}{2}} \rightarrow 4p_{\frac{1}{2}}$	$4s_{\frac{1}{2},-\frac{1}{2}} \rightarrow 4p_{\frac{1}{2},-\frac{1}{2}}$		$4s_{\frac{1}{2},\frac{1}{2}} \rightarrow 4p_{\frac{1}{2},\frac{1}{2}}$		$4s_{\frac{1}{2},-\frac{1}{2}} \rightarrow 4p_{\frac{1}{2},\frac{1}{2}}$		$4s_{\frac{1}{2},\frac{1}{2}} \rightarrow 4p_{\frac{1}{2},-\frac{1}{2}}$	
$4p_{\frac{1}{2}} \rightarrow 3d_{\frac{3}{2}}$	866.2									
		691.24(12.29)	778.37(6.39)	87.13	603.43(17.73)	−87.81	600.43(18.05)	−90.81	779.00(6.35)	87.76
$4s_{\frac{1}{2}} \rightarrow 4p_{\frac{1}{2}}$	396.8									
		395.1788(377)	395.5410(688)	0.3622	394.5839(41)	−0.5949			394.1570(227)	−1.0218
$4s_{\frac{1}{2}} \rightarrow 4p_{\frac{3}{2}}$	396.4									
$4p_{\frac{1}{2}} \rightarrow 5s_{\frac{1}{2}}$	370.6									
		368.0221(1412)			361.83(69)	−6.1921	362.38(67)	−5.64		
$4p_{\frac{1}{2}} \rightarrow 4d_{\frac{3}{2}}$	315.9									

caused by the incompleteness of the basis set used in actual calculations.

The present approach is based on the frozen-core model, in which an atom is partitioned into a core and valence electrons. We first perform a Dirac-Fock calculation on the ground state of the core. The orbitals of the core are expressed as linear combinations of S-spinors. Thereafter, valence electron wave functions are calculated by using a semiempirical-polarization-potential method. For atomic systems with a single valence electron, the effective interaction potential of the valence electron with the core is written as

$$H = c\boldsymbol{\alpha}\cdot\boldsymbol{p} + \beta c^2 + V_{\text{core}}(\boldsymbol{r}), \tag{1}$$

where $\boldsymbol{\alpha}$ and β denote 4×4 matrices of the Dirac operator, and $\boldsymbol{p}$ is the momentum operator of electrons [42]. Moreover, V_{core} represents the core interaction operator and is expressed as

$$V_{\text{core}}(\boldsymbol{r}) = -\frac{Z}{r} + V_{\text{dir}}(\boldsymbol{r}) + V_{\text{exc}}(\boldsymbol{r}) + V_{\text{p}}(\boldsymbol{r}). \tag{2}$$

TABLE II. Same as Table I but for the $4s_{\frac{1}{2},m} \rightarrow 4p_{\frac{3}{2},m'}$ transitions.

Resonances	λ_{res}	$\mathcal{A}=0$	$\mathcal{A}=-1$					
		λ_{magic}	λ_{magic}	$\Delta\lambda$	λ_{magic}	$\Delta\lambda$	λ_{magic}	$\Delta\lambda$	λ_{magic}	$\Delta\lambda$
		$4s_{\frac{1}{2}} \rightarrow 4p_{\frac{3}{2},\frac{1}{2}}$	$4s_{\frac{1}{2},-\frac{1}{2}} \rightarrow 4p_{\frac{3}{2},-\frac{1}{2}}$		$4s_{\frac{1}{2},\frac{1}{2}} \rightarrow 4p_{\frac{3}{2},\frac{1}{2}}$		$4s_{\frac{1}{2},-\frac{1}{2}} \rightarrow 4p_{\frac{3}{2},\frac{1}{2}}$		$4s_{\frac{1}{2},\frac{1}{2}} \rightarrow 4p_{\frac{3}{2},-\frac{1}{2}}$	
$4p_{\frac{3}{2}} \rightarrow 3d_{\frac{5}{2}}$	854.2									
		850.1164(1)	851.0555(21)	0.9391	850.4771(21)	0.3607	850.4770(6)	0.3606	851.0556(21)	0.9392
$4p_{\frac{3}{2}} \rightarrow 3d_{\frac{3}{2}}$	849.8									
		687.51(10.33)	722.97(10.35)	35.46	631.85(16.85)	−55.66	629.33(17.14)	−58.18	724.11(10.24)	36.6
$4s_{\frac{1}{2}} \rightarrow 4p_{\frac{1}{2}}$	396.8									
		396.2297(218)			394.5946(33)	−1.6351			395.1904(340)	−1.0393
$4s_{\frac{1}{2}} \rightarrow 4p_{\frac{3}{2}}$	393.4									
$4p_{\frac{3}{2}} \rightarrow 5s_{\frac{1}{2}}$	373.7									
		369.6523(1849)			370.30(26)	0.6477	370.57(24)	0.9177		
$4p_{\frac{3}{2}} \rightarrow 4d_{\frac{3}{2}}$	318.1									
		$4s_{\frac{1}{2}} \rightarrow 4p_{\frac{3}{2},\frac{3}{2}}$	$4s_{\frac{1}{2},-\frac{1}{2}} \rightarrow 4p_{\frac{3}{2},-\frac{3}{2}}$		$4s_{\frac{1}{2},\frac{1}{2}} \rightarrow 4p_{\frac{3}{2},\frac{3}{2}}$		$4s_{\frac{1}{2},-\frac{1}{2}} \rightarrow 4p_{\frac{3}{2},\frac{3}{2}}$		$4s_{\frac{1}{2},\frac{1}{2}} \rightarrow 4p_{\frac{3}{2},-\frac{3}{2}}$	
$4p_{\frac{3}{2}} \rightarrow 3d_{\frac{5}{2}}$	854.2									
		850.9217(15)	851.8764(65)	0.9547					851.8770(66)	0.9533
$4p_{\frac{3}{2}} \rightarrow 3d_{\frac{3}{2}}$	849.8									
		672.89(15.33)	803.96(3.39)	131.07	563.06(17.95)	−109.83	559.31(18.35)	−113.58	804.28(3.37)	131.39
$4p_{\frac{1}{2}} \rightarrow 4s_{\frac{1}{2}}$	396.8									
		395.7729(19)			394.5596(60)	−1.2133			395.7744(461)	0.0015
$4p_{\frac{3}{2}} \rightarrow 4s_{\frac{1}{2}}$	393.4									
					358.21(1.44)		359.25(1.42)			
$4p_{\frac{3}{2}} \rightarrow 4d_{\frac{3}{2}}$	318.1									

$V_{\rm dir}$ and $V_{\rm exc}$ represent direct and exchange interactions with core electrons [39], respectively. V_p is an extension of the semiempirical polarization potential. Such a core polarization potential is introduced to approximate the correlation interaction between the core and valence electrons [43]. V_p can be written as

$$V_{\rm p}(\mathbf{r}) = -\sum_{k=1}^{3} \frac{\alpha_{\rm core}^{(k)}}{2r^{[2(k+1)]}} \sum_{l,j} g_{k,l,j}^2(r)|l,j\rangle\langle l,j|, \tag{3}$$

where l and j are orbital and total angular momenta. The factors $\alpha_{\rm core}^{(k)}$ represent kth-order static polarizabilities of the core electrons. In our calculations, dipole polarizability $\alpha_{\rm core}^{(1)}$ of the core is taken as 3.26 a.u., quadrupole polarizability $\alpha_{\rm core}^{(2)}$ is 6.9 a.u., and octupole polarizability $\alpha_{\rm core}^{(3)}$ is 34 a.u. [44]. $g_{k,l,j}^2(r)$ is a cutoff function designed to make the polarization potential finite at the origin, which has the form $g_{k,l,j}^2(r) = 1 - \exp[-r^{[2(k+2)]}/\rho_{l,j}^{[2(k+2)]}]$ [39]. The cutoff parameters $\rho_{l,j}$ that are tuned to reproduce binding energies of the corresponding states are listed in Supplemental Material, Table I [45]. The effective Hamiltonian for the valence electrons was diagonalized in a large S-spinor and L-spinor basis. The present RCICP calculations typically used 35 positive-energy and 35 negative-energy L-spinors for each (l, j) symmetry.

For an arbitrarily polarized light, the dynamic polarizability for an atomic state i is given by [22,46,47]

$$\alpha_i(\omega) = \alpha_i^S(\omega) + \mathcal{A}\cos\theta_k \frac{m_{j_i}}{2j_i}\alpha_i^V(\omega) + \left(\frac{3\cos^2\theta_p - 1}{2}\right)\frac{3m_{j_i}^2 - j_i(j_i+1)}{j_i(2j_i-1)}\alpha_i^T(\omega), \tag{4}$$

where $\alpha_i^S(\omega)$, $\alpha_i^V(\omega)$, and $\alpha_i^T(\omega)$ represent the scalar, vector, and tensor polarizabilities for the state i, respectively; m_{j_i} is the component of the total angular momentum j_i. It is noted that there is no tensor polarizability for the states with $j \leqslant \frac{1}{2}$. θ_k is the angle between the wave vector and z axis as defined below. θ_p relates to the polarization vector and z axis. It is obtained from a geometrical consideration that θ_k and θ_p satisfy the relation $\cos^2\theta_k + \cos^2\theta_p \leqslant 1$ [22,46]. $\mathcal{A}$ represents the degree of polarization. For linearly polarized light, $\mathcal{A} = 0$, and thus we choose the polarization vector as the z axis, which is perpendicular to the wave vector. In this case, $\cos\theta_k = 0$ and $\cos\theta_p = 1$, which simplify Eq. (4) to

$$\alpha_i(\omega) = \alpha_i^S(\omega) + \frac{3m_{j_i}^2 - j_i(j_i+1)}{j_i(2j_i-1)}\alpha_i^T(\omega). \tag{5}$$

However, for circularly polarized light ($\mathcal{A} = 1$ for the right-handed and -1 for the left-handed), the z axis is chosen along the wave vector. As a consequence, $\cos\theta_k = 1$ and $\cos^2\theta_p = 0$. Equation (4) is thus simplified as

$$\alpha_i(\omega) = \alpha_i^S(\omega) + \mathcal{A}\frac{m_{j_i}}{2j_i}\alpha_i^V(\omega) - \frac{3m_{j_i}^2 - j_i(j_i+1)}{2j_i(2j_i-1)}\alpha_i^T(\omega). \tag{6}$$

Equation (6) can also be written as

$$\alpha_i(\omega) = \sum_n F_{i,n}^S(\omega) + \mathcal{A}\sum_n F_{i,n}^V(\omega) + \sum_n F_{i,n}^T(\omega), \tag{7}$$

where the factors $F_{i,n}^S(\omega)$, $F_{i,n}^V(\omega)$, and $F_{i,n}^T(\omega)$ characterize, respectively, the scalar, vector, and tensor contributions to the polarizability, and are defined as

$$F_{i,n}^S(\omega) = \frac{f_{i,n}}{\Delta E_{i,n}^2 - \omega^2}, \tag{8}$$

$$F_{i,n}^V(\omega) = -\frac{3m_{j_i}}{2j_i}\sqrt{\frac{6j_i(2j_i+1)}{(j_i+1)}}\begin{Bmatrix} 1 & 1 & 1 \\ j_i & j_i & j_n \end{Bmatrix} \times (-1)^{j_i+j_n}\frac{f_{i,n}}{\Delta E_{i,n}^2 - \omega^2}\frac{\omega}{\Delta E_{i,n}}, \tag{9}$$

and

$$F_{i,n}^T(\omega) = -\frac{3m_{j_i}^2 - j_i(j_i+1)}{2j_i(2j_i-1)} \times 6\sqrt{\frac{5j_i(2j_i-1)(2j_i+1)}{6(j_i+1)(2j_i+3)}} \times \begin{Bmatrix} 1 & 1 & 2 \\ j_i & j_i & j_n \end{Bmatrix}(-1)^{j_i+j_n}\frac{f_{i,n}}{\Delta E_{i,n}^2 - \omega^2}. \tag{10}$$

In these expressions, $\Delta E_{i,n}$ is the transition energy from state n to state i. Dipole absorption oscillator strength $f_{i,n}$ is defined as

$$f_{i,n} = \frac{2\Delta E_{i,n}|\langle\psi_i\|rC^{(1)}(\hat{\mathbf{r}})\|\psi_n\rangle|^2}{3(2j_i+1)}, \tag{11}$$

where $C^{(1)}(\hat{\mathbf{r}})$ is the first-order spherical tensor.

TABLE III. The contributions of individual transitions to the polarizabilities (in a.u.) of the $4s_{\frac{1}{2},\pm\frac{1}{2}}$ and $4p_{\frac{3}{2},\pm\frac{1}{2}}$ states at the magic wavelengths. These results are calculated for left-handed polarized light.

		$\mathcal{A}=-1$	
ω (a.u.)	0	0.05357388	0.05353745
λ (nm)	∞	850.4770(6)	851.0556(21)
		$4s_{\frac{1}{2},-\frac{1}{2}}$	$4s_{\frac{1}{2},+\frac{1}{2}}$
$4p_{\frac{1}{2}}$	24.1492	16.4645	45.2599
$4p_{\frac{3}{2}}$	47.9069	75.0544	46.8459
$5p_{\frac{1}{2}}$	0.0091	0.0076	0.0113
$5p_{\frac{3}{2}}$	0.0135	0.0154	0.0126
Remains	0.2261	0.2280	0.2292
Core	3.1596	3.1635	3.1635
Total	75.4644	94.9333	95.5224
		$4p_{\frac{3}{2},+\frac{1}{2}}$	$4p_{\frac{3}{2},-\frac{1}{2}}$
$4s_{\frac{1}{2}}$	−47.9069	−8.1883	−22.2757
$3d_{\frac{3}{2}}$	−0.7769	−4491.7847	−2593.9354
$3d_{\frac{5}{2}}$	−42.3461	4534.9763	2649.1186
$5s_{\frac{1}{2}}$	24.1915	10.7904	4.2022
$4d_{\frac{3}{2}}$	0.8356	7.1650	6.4367
$4d_{\frac{5}{2}}$	45.0045	34.3492	44.1184
$6s_{\frac{1}{2}}$	1.1309	0.3820	0.2245
$5d_{\frac{3}{2}}$	0.0489	0.3775	0.3516
$5d_{\frac{5}{2}}$	2.6432	1.9378	2.2875
Remains	2.6896	1.7648	1.8306
Core	3.1596	3.1635	3.1635
Total	−11.3262	94.9333	95.5224

TABLE IV. The contributions of individual transitions to the polarizabilities (in a.u.) of the $4s_{\frac{1}{2},\pm\frac{1}{2}}$ and $4p_{\frac{3}{2},-\frac{3}{2}}$ states for left-handed polarized light at the corresponding magic wavelengths. $\sum$ represents the sum of F^S, $\mathcal{A}\mathrm{F}^V$, and F^T.

	$\lambda_{\mathrm{magic}} = 851.8770$ (nm) $\omega_1 = 0.053485833$ (a.u.)				$\lambda_{\mathrm{magic}} = 851.8764$ (nm) $\omega_2 = 0.053485871$ (a.u.)			
	F^S	$\mathcal{A}\mathrm{F}^V$	F^T	$\sum$	F^S	$\mathcal{A}\mathrm{F}^V$	F^T	$\sum$
	$4s_{\frac{1}{2},+\frac{1}{2}}$				$4s_{\frac{1}{2},-\frac{1}{2}}$			
$4p_{\frac{1}{2}}$	30.8474	14.3743		45.2218	30.8474	−14.3744		16.4731
$4p_{\frac{3}{2}}$	60.8996	−14.0646		46.8350	60.8996	14.0646		74.9642
$5p_{\frac{1}{2}}$	0.0094	0.0018		0.0113	0.0094	−0.0018		0.0076
$5p_{\frac{3}{2}}$	0.0140	−0.0014		0.0126	0.0140	0.0014		0.0154
Remains	0.2286	0.0006		0.2292	0.2286	−0.0006		0.2280
Core	3.1635	0.0000		3.1635	3.1635	0.0000		3.1635
Total	95.1625	0.3108		95.4733	95.1626	−0.3108		94.8518
	$4p_{\frac{3}{2},-\frac{3}{2}}$				$4p_{\frac{3}{2},-\frac{3}{2}}$			
$4s_{\frac{1}{2}}$	−30.4498	−21.0969	−15.2249	−66.7716	−30.4498	−21.0969	−15.2249	−66.7716
$3d_{\frac{3}{2}}$	−899.4967	−538.5314	359.7987	−1078.2295	−899.7872	−538.7057	359.9149	−1078.5780
$3d_{\frac{5}{2}}$	5848.5182	−5279.5223	584.8518	1153.8477	5847.1531	−5278.2937	584.7153	1153.5747
$5s_{\frac{1}{2}}$	14.9799	−9.8596	7.4900	12.6103	14.9799	−9.8596	7.4900	12.6103
$4d_{\frac{3}{2}}$	4.8556	−1.0883	−1.9422	1.8251	4.8556	−1.0883	−1.9422	1.8251
$4d_{\frac{5}{2}}$	43.5771	14.6415	4.3577	62.5763	43.5771	14.6415	4.3577	62.5763
$6s_{\frac{1}{2}}$	0.6062	−0.2358	0.3031	0.6735	0.6062	−0.2358	0.3031	0.6735
$5d_{\frac{3}{2}}$	0.2604	−0.0388	−0.1041	0.1174	0.2604	−0.0388	−0.1041	0.1174
$5d_{\frac{5}{2}}$	2.3471	0.5241	0.2347	3.1059	2.3471	0.5241	0.2347	3.1059
Remains	2.1268	0.0987	0.3292	2.5548	2.1268	0.0987	0.3292	2.5548
Core	3.1635	0.0000	0.0000	3.1635	3.1635	0.0000	0.0000	3.1635
Total	4990.4882	−5835.1088	940.0940	95.4733	4988.8326	−5834.0546	940.0737	94.8518

III. RESULTS AND DISCUSSION

For illustrating the accuracy of the present calculations, the energy levels, electric-dipole matrix elements, static polarizabilities, and magic wavelength of Ca^+ ions are calculated for linearly polarized light, which are compared with existing theoretical and experimental results [14,15,48]. Good agreements among them are found (see Supplemental Material, Tables II–V [45]). For instance, the scalar polarizabilities of the $4s_{\frac{1}{2}}$, $3d_{\frac{3}{2}}$, and $3d_{\frac{5}{2}}$ states are determined to be 75.46, 32.98, and 32.80 a.u. in the present calculations, as compared to the many-body perturbation theory results of 76.1, 32.0, and 32.0 a.u. [44], respectively. In the following, we just consider the case of circularly polarized light.

The dynamic polarizability is different for each of the magnetic sublevels of an atomic level. According to Eq. (6), the dynamic polarizabilities of atomic states with negative m for $\mathcal{A} = -1$ are the same as the ones of states with positive m for $\mathcal{A} = +1$. For this reason, we give the polarizabilities of the $4s_{\frac{1}{2},m}$, $4p_{j,m}$, and $3d_{j,m}$ states just for left-handed polarized light in the following discussions.

In order to find the magic wavelengths for all of the transitions between the $4s_{\frac{1}{2},m}$ and $4p_{\frac{1}{2},m'}$ states, Fig. 1 shows the dynamic polarizabilities of these states, which are plotted for different pairs of their initial and final states. In Fig. 1(a), for instance, we give the polarizabilities of the $4s_{\frac{1}{2},-\frac{1}{2}}$ and $4p_{\frac{1}{2},-\frac{1}{2}}$ states. As can be seen clearly from Fig. 2, the behaviors of the dynamic polarizabilities of the $4s_{\frac{1}{2},-\frac{1}{2}}$ state are different from the case of linearly polarized light. When the laser wavelength is close to the $4s \to 4p_{\frac{1}{2}}$ transition, $\alpha_{4s} \to \infty$ for linearly polarized light. For left-handed polarized light ($\mathcal{A} = -1$), however, the polarizabilities of the $4s_{\frac{1}{2},-\frac{1}{2}}$ state remain finite as seen in Fig. 2. This is because the $4s \to 4p_{\frac{1}{2}}$ transition does not contribute to the polarizability when the wavelength is close to the $4s \to 4p_{\frac{1}{2}}$ transition. To be more specific, the contributions of the scalar and vector terms from the $4s \to 4p_{\frac{1}{2}}$ transition cancel each other out, while its tensor term does not exist, i.e.,

$$\lim_{\omega \to \Delta E_{i,4p_{\frac{1}{2}}}} \left(F^S_{i,4p_{\frac{1}{2}}} - F^V_{i,4p_{\frac{1}{2}}}\right) = 0, \tag{12}$$

where i represents the $4s_{\frac{1}{2},-\frac{1}{2}}$ state. A similar behavior occurs also for the polarizabilities of the $4p_{\frac{1}{2},-\frac{1}{2}}$ state but when the wavelength is close to the $4p_{\frac{1}{2}} \to 5s_{\frac{1}{2}}$ transition. The intersections of the dynamic polarizabilities of the $4s_{\frac{1}{2},-\frac{1}{2}}$ and $4p_{\frac{1}{2},-\frac{1}{2}}$ states give rise to magic wavelengths, which are pointed out by arrows.

Table I lists the obtained magic wavelengths of the $4s_{\frac{1}{2},m} \to 4p_{\frac{1}{2},m'}$ transitions together with the ones of the $4s_{\frac{1}{2}} \to 4p_{\frac{1}{2}}$ transition for linearly polarized light for comparison. The differences of the magic wavelengths between the two kinds of polarization are also given. For each of the transitions, two or three magic wavelengths are found in the range of 300 to 1000 nm. Take the $4s_{\frac{1}{2},-\frac{1}{2}} \to 4p_{\frac{1}{2},-\frac{1}{2}}$ transition, for example,

TABLE V. Same as Table I but for the $4s_{\frac{1}{2},m} \rightarrow 3d_{\frac{3}{2},m'}$ and $4s_{\frac{1}{2},m} \rightarrow 3d_{\frac{5}{2},m'}$ transitions.

Resonances λ_{res}	$\mathcal{A}=0$	$\mathcal{A}=-1$							
	λ_{magic}	λ_{magic}	$\Delta\lambda$	λ_{magic}	$\Delta\lambda$	λ_{magic}	$\Delta\lambda$	λ_{magic}	$\Delta\lambda$
	$4s_{\frac{1}{2}} \rightarrow 3d_{\frac{3}{2},\frac{3}{2}}$	$4s_{\frac{1}{2},-\frac{1}{2}} \rightarrow 3d_{\frac{3}{2},-\frac{3}{2}}$		$4s_{\frac{1}{2},\frac{1}{2}} \rightarrow 3d_{\frac{3}{2},\frac{3}{2}}$		$4s_{\frac{1}{2},-\frac{1}{2}} \rightarrow 3d_{\frac{3}{2},\frac{3}{2}}$		$4s_{\frac{1}{2},\frac{1}{2}} \rightarrow 3d_{\frac{3}{2},-\frac{3}{2}}$	
	887.28(3.52)			1580.01(142.74)	692.73	1584.95(143.70)	697.67		
				1467.8(4) [38]		1549.9(5) [38]			
$3d_{\frac{3}{2}} \rightarrow 4p_{\frac{1}{2}}$ 866.2									
				851.1724(42)		851.1728(42)			
				850.9(2) [38]		851.2(3) [38]			
$4s_{\frac{1}{2}} \rightarrow 4p_{\frac{1}{2}}$ 396.8									
	395.7951(1)			394.6394(4)	−1.1557			394.6315(2)	−1.1636
				394.6(9) [38]				394.6(10) [38]	
$4s_{\frac{1}{2}} \rightarrow 4p_{\frac{3}{2}}$ 393.4									
	$4s_{\frac{1}{2}} \rightarrow 3d_{\frac{3}{2},\frac{1}{2}}$	$4s_{\frac{1}{2},-\frac{1}{2}} \rightarrow 3d_{\frac{3}{2},-\frac{1}{2}}$		$4s_{\frac{1}{2},\frac{1}{2}} \rightarrow 3d_{\frac{3}{2},\frac{1}{2}}$		$4s_{\frac{1}{2},-\frac{1}{2}} \rightarrow 3d_{\frac{3}{2},\frac{1}{2}}$		$4s_{\frac{1}{2},\frac{1}{2}} \rightarrow 3d_{\frac{3}{2},-\frac{1}{2}}$	
	1307.60(96.2)	876.28(2.61)	−431.32	1035.46(20.15)	−271.14	1036.70(20.30)	−270.9	876.07(2.59)	−431.53
		875.56(2) [38]		1013.4(5) [38]		1031.4(4) [38]		870.7(3) [38]	
$3d_{\frac{3}{2}} \rightarrow 4p_{\frac{1}{2}}$ 866.2									
	850.3301(18)			853.5974(266)	3.2673	853.5998(264)	3.2697		
				853.1(2) [38]		853.5(4) [38]			
$3d_{\frac{3}{2}} \rightarrow 4p_{\frac{3}{2}}$ 849.8									
$4s_{\frac{1}{2}} \rightarrow 4p_{\frac{1}{2}}$ 396.8									
	395.7962(1)			394.6362(1)	−1.16			394.6335(1)	−1.1627
				394.6(9) [38]				394.6(10) [38]	
$4s_{\frac{1}{2}} \rightarrow 4p_{\frac{3}{2}}$ 393.4									
	$4s_{\frac{1}{2}} \rightarrow 3d_{\frac{5}{2},\frac{5}{2}}$	$4s_{\frac{1}{2},-\frac{1}{2}} \rightarrow 3d_{\frac{5}{2},-\frac{5}{2}}$		$4s_{\frac{1}{2},\frac{1}{2}} \rightarrow 3d_{\frac{5}{2},\frac{5}{2}}$		$4s_{\frac{1}{2},-\frac{1}{2}} \rightarrow 3d_{\frac{5}{2},\frac{5}{2}}$		$4s_{\frac{1}{2},\frac{1}{2}} \rightarrow 3d_{\frac{5}{2},-\frac{5}{2}}$	
				1726.68(198.7)		1732.77(200.04)			
$4s_{\frac{1}{2}} \rightarrow 4p_{\frac{1}{2}}$ 396.8									
	395.7949(1)			394.6400(4)	−1.1549			394.6311(3)	−1.1638
				394.64(2) [38]				394.63(3) [38]	
$4s_{\frac{1}{2}} \rightarrow 4p_{\frac{3}{2}}$ 393.4									
	$4s_{\frac{1}{2}} \rightarrow 3d_{\frac{5}{2},\frac{3}{2}}$	$4s_{\frac{1}{2},-\frac{1}{2}} \rightarrow 3d_{\frac{5}{2},-\frac{3}{2}}$		$4s_{\frac{1}{2},\frac{1}{2}} \rightarrow 3d_{\frac{5}{2},\frac{3}{2}}$		$4s_{\frac{1}{2},-\frac{1}{2}} \rightarrow 3d_{\frac{5}{2},\frac{3}{2}}$		$4s_{\frac{1}{2},\frac{1}{2}} \rightarrow 3d_{\frac{5}{2},-\frac{3}{2}}$	
	1073.80(31.61)			1185.07(46.46)	111.27	1187.42(46.79)	113.62		
				1150.39(2) [38]		1173.5(2) [38]			
$3d_{\frac{5}{2}} \rightarrow 4p_{\frac{3}{2}}$ 854.2									
$4s_{\frac{1}{2}} \rightarrow 4p_{\frac{1}{2}}$ 396.8									
	395.7958(1)			394.6377(2)	−1.1581			394.6324(2)	−1.1634
				394.64(3) [38]				394.63(3) [38]	
$4s_{\frac{1}{2}} \rightarrow 4p_{\frac{3}{2}}$ 393.4									
	$4s_{\frac{1}{2}} \rightarrow 3d_{\frac{5}{2},\frac{1}{2}}$	$4s_{\frac{1}{2},-\frac{1}{2}} \rightarrow 3d_{\frac{5}{2},-\frac{1}{2}}$		$4s_{\frac{1}{2},\frac{1}{2}} \rightarrow 3d_{\frac{5}{2},\frac{1}{2}}$		$4s_{\frac{1}{2},-\frac{1}{2}} \rightarrow 3d_{\frac{5}{2},\frac{1}{2}}$		$4s_{\frac{1}{2},\frac{1}{2}} \rightarrow 3d_{\frac{5}{2},-\frac{1}{2}}$	
	1337.30(115.38)	894.81(4.06)	−442.49	986.63(14.76)	−350.67	987.60(14.87)	−349.7	894.50(4.03)	−442.8
		893.4(3) [38]		975.6(4) [38]		982.7(2) [38]		891.4(3) [38]	
$3d_{\frac{5}{2}} \rightarrow 4p_{\frac{3}{2}}$ 854.2									
$4s_{\frac{1}{2}} \rightarrow 4p_{\frac{1}{2}}$ 396.8									
	395.7963(1)			394.6357(1)	−1.1606			394.6339(1)	−1.1624
				394.64(2) [38]				394.63(4) [38]	
$4s_{\frac{1}{2}} \rightarrow 4p_{\frac{3}{2}}$ 393.4									

which has two magic wavelengths. One is 395.5410 nm, which lies between the $4s_{\frac{1}{2}} \rightarrow 4p_{\frac{1}{2}}$ and $4s_{\frac{1}{2}} \rightarrow 4p_{\frac{3}{2}}$ transition wavelengths. This magic wavelength is very close to the 395.1788-nm one for the case of linearly polarized light. The difference is only 0.3622 nm. Another one is 778.37 nm that occurs between the $4p_{\frac{1}{2}} \rightarrow 4s$ and $4p_{\frac{1}{2}} \rightarrow 3d_{\frac{3}{2}}$ transition energies. In contrast, this magic wavelength has 87-nm difference from the magic wavelength 691.24 nm for the $4s \rightarrow 4p_{\frac{1}{2}}$ transition in the case of linearly polarized light.

Table II lists the magic wavelengths of the $4s_{\frac{1}{2},m} \rightarrow 4p_{\frac{3}{2},m'}$ transitions, which are obtained from the corresponding dynamic polarizabilities as shown in Supplemental Material, Figs. 2 and 3 [45]. Much attention should be paid to the

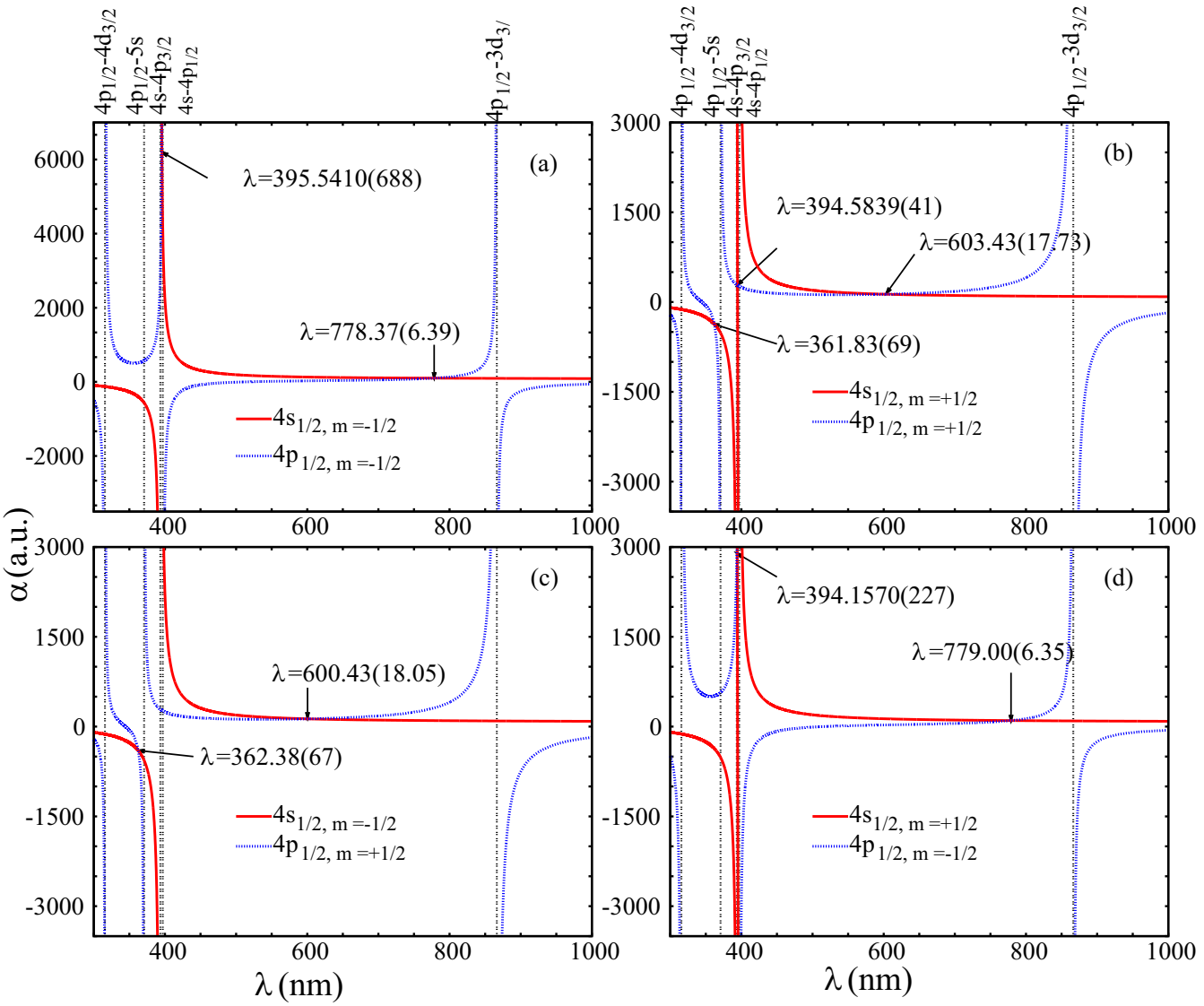

FIG. 1. Dynamic polarizabilities for the $4s_{\frac{1}{2},\pm\frac{1}{2}}$ and $4p_{\frac{1}{2},\pm\frac{1}{2}}$ states of Ca^+ for left-handed circularly polarized light. (a–d) The $4s_{\frac{1}{2},-\frac{1}{2}} \rightarrow 4p_{\frac{1}{2},-\frac{1}{2}}$, $4s_{\frac{1}{2},+\frac{1}{2}} \rightarrow 4p_{\frac{1}{2},+\frac{1}{2}}$, $4s_{\frac{1}{2},-\frac{1}{2}} \rightarrow 4p_{\frac{1}{2},+\frac{1}{2}}$, and $4s_{\frac{1}{2},+\frac{1}{2}} \rightarrow 4p_{\frac{1}{2},-\frac{1}{2}}$ transitions, respectively. The obtained magic wavelengths are illustrated by arrows. The vertical lines identify the resonance transition wavelengths.

magic wavelengths near 851 nm, since these wavelengths arise due to a cancellation in the polarizabilities from two transitions of $4p_{\frac{3}{2}} \rightarrow 3d_j$ spin-orbital splitting. Table III gives the contributions of individual transitions to the polarizabilities of the $4s_{\frac{1}{2},m}$ $(m = \pm\frac{1}{2})$ and $4p_{\frac{3}{2},m'}$ $(m' = \pm\frac{1}{2})$ states at the magic wavelengths. The notation "Remains" includes the contributions of highly excited bound and continuum states of the valence electrons. The notation "Core" denotes the contributions from the excitations of core electrons. It can be found that the $4s_{\frac{1}{2},m}$ polarizability is dominated by the $4s_{\frac{1}{2}} \rightarrow 4p_j$ transitions and the $4p_{\frac{3}{2},m'}$ polarizability is dominated by the $4p_{\frac{3}{2}} \rightarrow 3d_j$ transitions. With the use of the experimental matrix elements of the $4s_{\frac{1}{2}} \rightarrow 4p_j$ transitions, the measurement of these magic wavelengths can be used to determine the ratio of the oscillator strengths for the $4p_{\frac{3}{2}} \rightarrow 3d_{\frac{3}{2}}$ and $4p_{\frac{3}{2}} \rightarrow 3d_{\frac{5}{2}}$ transitions. Supposing that all the remaining components (including the $4p_{\frac{3}{2}} \rightarrow 5s_{\frac{1}{2}}$ and $4d_j$ contributions) of the $4p_{\frac{3}{2}}$ polarizability are estimated with an accuracy of 5%, the overall uncertainty of the polarizability is less than 1%.

It also can be seen that the difference of the magic wavelengths 851.8770 and 851.8764 nm for the $4s_{\frac{1}{2},\frac{1}{2}} \rightarrow 4p_{\frac{3}{2},-\frac{3}{2}}$ and $4s_{\frac{1}{2},-\frac{1}{2}} \rightarrow 4p_{\frac{3}{2},-\frac{3}{2}}$ transitions is just 0.0006 nm, which could be resolved in present-day experiments [14,26,30]. By performing high-precision measurements on these two magic wavelengths, the ratio of the oscillator strengths for the $4p_{\frac{3}{2}} \rightarrow 3d_{\frac{3}{2}}$ and $4p_{\frac{3}{2}} \rightarrow 3d_{\frac{5}{2}}$ transitions can be determined with very high accuracy. To further explain this, Table IV tabulates the contributions to the polarizabilities of the corresponding states at the magic wavelengths 851.8770 nm ($\omega_1 = 0.053485833$ a.u.) and 851.8764 nm ($\omega_2 = 0.053485871$ a.u.). At these two magic wavelengths

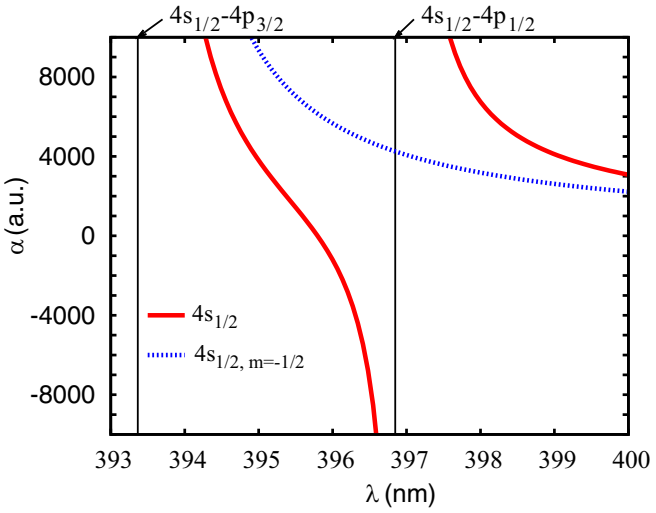

FIG. 2. Dynamic polarizabilities for the $4s_{\frac{1}{2},-\frac{1}{2}}$ state of Ca^+ in the wavelength range 393–400 nm for linearly ($\mathcal{A}=0$, red solid line) and left-handed circularly ($\mathcal{A}=-1$, blue dotted line) polarized light. The approximate positions of the $4s_{\frac{1}{2}} \rightarrow 4p_j$ resonances are indicated by vertical lines.

(frequencies),

$$\alpha_{4p_{\frac{3}{2},-\frac{3}{2}}}(\omega_1) = \alpha_{4s_{\frac{1}{2},\frac{1}{2}}}(\omega_1), \tag{13}$$

$$\alpha_{4p_{\frac{3}{2},-\frac{3}{2}}}(\omega_2) = \alpha_{4s_{\frac{1}{2},-\frac{1}{2}}}(\omega_2). \tag{14}$$

Using Eq. (7) and the numbers in Table IV, the subtraction of Eq. (13) from Eq. (14) gives rise to

$$C_1 f_{4p_{\frac{3}{2}},3d_{\frac{3}{2}}} + C_2 f_{4p_{\frac{3}{2}},3d_{\frac{5}{2}}} \approx \alpha^V_{4s_{\frac{1}{2}}}(\omega_1), \tag{15}$$

where

$$C_1 = \frac{3}{5}\left(\frac{1}{\Delta E^2_{i,b}-\omega_1^2} - \frac{1}{\Delta E^2_{i,b}-\omega_2^2}\right) - \frac{3}{5\Delta E_{i,b}}\left(\frac{\omega_1}{\Delta E^2_{i,b}-\omega_1^2} - \frac{\omega_2}{\Delta E^2_{i,b}-\omega_2^2}\right), \tag{16}$$

$$C_2 = \frac{11}{10}\left(\frac{1}{\Delta E^2_{i,q}-\omega_1^2} - \frac{1}{\Delta E^2_{i,q}-\omega_2^2}\right) + \frac{9}{10\Delta E_{i,q}}\left(\frac{\omega_1}{\Delta E^2_{i,q}-\omega_1^2} - \frac{\omega_2}{\Delta E^2_{i,q}-\omega_2^2}\right). \tag{17}$$

In these expressions, i, b, and q represent the $4p_{\frac{3}{2}}$, $3d_{\frac{3}{2}}$, and $3d_{\frac{5}{2}}$ states, respectively. In Eq. (15), once the vector polarizability $\alpha^V_{4s_{\frac{1}{2}}}(\omega_1)$ is determined, the measurement on the magic wavelengths ω_1 and ω_2 can give the ratio of the oscillator strengths for the $4p_{\frac{3}{2}} \rightarrow 3d_{\frac{3}{2}}$ and $4p_{\frac{3}{2}} \rightarrow 3d_{\frac{5}{2}}$ transitions. Actually, the main contribution of $\alpha^V_{4s_{\frac{1}{2}}}(\omega_1)$ comes from the $4p_j$ and $5p_j$ states, and reaches 99.77% as seen from Table IV and can be determined very accurately [14].

The magic wavelengths for the $4s_{\frac{1}{2},\pm\frac{1}{2}}$ and $3d_{j,m}$ states are listed in Table V and compared with the results from a very recent work [38] performed with the use of a relativistic coupled-cluster (RCC) method. Good consistency is obtained for the magic wavelengths shorter than 1000 nm. For example, the differences of the magic wavelengths near 394.6 nm between the present RCICP calculations and the RCC results [38] are less than 0.01%. However, the magic wavelengths longer than 1000 nm have a big difference. For instance, the present magic wavelength 1580.01 nm of the transition $4s_{\frac{1}{2},\frac{1}{2}} \rightarrow 3d_{\frac{3}{2},\frac{3}{2}}$ is longer by 112.21 nm than the RCC result 1467.8 nm. One reason is that the static polarizabilities of the $4s$ and $3d_j$ states have about 2% differences between the RCICP and the RCC [38] results, as can be seen in Supplemental Material, Table IV [45]. Another one is that the polarizabilities of the $4s_{\frac{1}{2},m}$ and $3d_{j',m'}$ states change slowly with the wavelengths longer than 1000 nm as can be seen in Supplemental Material, Figs. 4 and 5 [45]. It should be noted that the uncertainties of these magic wavelengths were estimated less than 0.5 nm in Ref. [38]. We believe these uncertainties were improperly estimated as the uncertainty of the static polarizability of $3d_j$ is as large as 1.8 a.u. (5.4%) in Ref. [38].

We found that the magic wavelengths near 394.6 nm lie between the $4s \rightarrow 4p_j$ resonant transitions which are smaller by about 1 nm than 395.79 nm of the $4s \rightarrow 3d_{j,m}$ transitions for linearly polarized light. The measurements on the magic wavelengths near 394.6 nm can be used as an additional tool for determining the ratio of the oscillator strengths for the $4s \rightarrow 4p_j$ transitions. Moreover, the measurement of magic wavelengths near 851 nm for $4s_{\frac{1}{2},m} \rightarrow 3d_{\frac{3}{2},m'}$ can be used to determine the ratio of the oscillator strengths for the $3d_{\frac{3}{2}} \rightarrow 4p_{\frac{1}{2}}$ and $3d_{\frac{3}{2}} \rightarrow 4p_{\frac{3}{2}}$ transitions. Supplemental Material, Tables XI–XXI list the individual transitions contributions of the polarizabilities at the magic wavelengths [45].

IV. CONCLUSIONS

The dynamic dipole polarizabilities of the $4s$, $4p_j$, and $3d_j$ states of Ca^+ ions are calculated for linearly and circularly polarized light. The magic wavelengths are determined for each of the magnetic sublevel transitions $4s_{j,m} \rightarrow 4p_{j',m'}$ and $4s_{j,m} \rightarrow 3d_{j',m'}$. The magic wavelengths for linearly polarized light agree very well with the available results [13,15]. Moreover, the magic wavelengths for circularly polarized light also agree with very recent theoretical results for the magic wavelengths shorter than 1000 nm, but the magic wavelengths longer than 1000 nm have a big difference [38]. We suggest that the measurement on the magic wavelength near 851 nm for the $4s_{\frac{1}{2},m} \rightarrow 4p_{\frac{3}{2},m'}(m=\pm\frac{3}{2},\pm\frac{1}{2})$ transitions can be used to determine the ratio of the oscillator strengths for the $3d_{\frac{3}{2}} \rightarrow 4p_{\frac{3}{2}}$ and $4p_{\frac{3}{2}} \rightarrow 3d_{\frac{5}{2}}$ transitions.

ACKNOWLEDGMENTS

We would like to thank Dr. Z. W. Wu and Dr. P. Shaw for helpful discussions and the anonymous referee for their valuable suggestions. The work of J.J. was supported by National Natural Science Foundation of China (NSFC) (Grants No. 11564036 and No. 11774292). The work of L.Y.X. was supported by NSFC (Grant No. U1331122). The work of D.H.Z. was supported by NSFC (Grants No. 11464042 and No. U1330117). The work of C.Z.D. was supported by NSFC (Grants No. 11274254 and No. U1332206).

[1] J. Ye, D. W. Vernooy, and H. J. Kimble, Phys. Rev. Lett. **83**, 4987 (1999).

[2] H. Katori, T. Ido, and M. K. Gonokami, J. Phys. Soc. Jpn. **68**, 2479 (1999).

[3] M. Takamoto and H. Katori, Phys. Rev. Lett. **91**, 223001 (2003).

[4] A. Bauch, Meas. Sci. Technol. **14**, 1159 (2003).

[5] P. Gill, G. P. Barwood, H. A. Klein, G. Huang, S. A. Webster, P. J. Blythe, K. Hosaka, S. N. Lea, and H. S. Margolis, Meas. Sci. Technol. **14**, 1174 (2003).

[6] P. Gill, Metrologia **42**, S125 (2005).

[7] L. Lorini, N. Ashby, A. Brusch, S. Diddams, R. Drullinger, E. Eason, T. Fortier, P. Hastings, T. Heavner, D. Hume *et al.*, Eur. Phys. J. Spec. Top. **163**, 19 (2008).

[8] P. Gill, Phil. Trans. R. Soc. A **369**, 4109 (2011).

[9] G. Kirchmair, J. Benhelm, F. Zähringer, R. Gerritsma, C. F. Roos, and R. Blatt, Phys. Rev. A **79**, 020304(R) (2009).

[10] B. K. Sahoo and B. Arora, Phys. Rev. A **87**, 023402 (2013).

[11] G. Wilpers, C. W. Oates, S. A. Diddams, A. Bartels, T. M. Fortier, W. H. Oskay, J. C. Bergquist, S. R. Jefferts, T. P. Heavner, T. E. Parker *et al.*, Metrologia **44**, 146 (2007).

[12] A. D. Ludlow, T. Zelevinsky, G. K. Campbell, S. Blatt, M. M. Boyd, M. H. de Miranda, M. J. Martin, J. W. Thomsen, S. M. Foreman, and J. Ye, Science **319**, 1805 (2008).

[13] J. Kaur, S. Singh, B. Arora, and B. K. Sahoo, Phys. Rev. A **92**, 031402(R) (2015).

[14] P.-L. Liu, Y. Huang, W. Bian, H. Shao, H. Guan, Y.-B. Tang, C.-B. Li, J. Mitroy, and K.-L. Gao, Phys. Rev. Lett. **114**, 223001 (2015).

[15] Y.-B. Tang, H.-X. Qiao, T.-Y. Shi, and J. Mitroy, Phys. Rev. A **87**, 042517 (2013).

[16] N. Lundblad, M. Schlosser, and J. V. Porto, Phys. Rev. A **81**, 031611(R) (2010).

[17] B. Arora, M. S. Safronova, and C. W. Clark, Phys. Rev. A **76**, 064501 (2007).

[18] S. Singh, B. K. Sahoo, and B. Arora, Phys. Rev. A **94**, 023418 (2016).

[19] K. L. Corwin, S. J. M. Kuppens, D. Cho, and C. E. Wieman, Phys. Rev. Lett. **83**, 1311 (1999).

[20] C. Cohen-Tannoudji and J. Dupont-Roc, Phys. Rev. A **5**, 968 (1972).

[21] C. Y. Park, H. Noh, C. M. Lee, and D. Cho, Phys. Rev. A **63**, 032512 (2001).

[22] F. Le Kien, P. Schneeweiss, and A. Rauschenbeutel, Eur. Phys. J. D **67**, 92 (2013).

[23] B. Arora and B. K. Sahoo, Phys. Rev. A **86**, 033416 (2012).

[24] S. Singh, B. K. Sahoo, and B. Arora, Phys. Rev. A **93**, 063422 (2016).

[25] S. Singh, K. Kaur, B. K. Sahoo, and B. Arora, J. Phys. B **49**, 145005 (2016).

[26] W. F. Holmgren, R. Trubko, I. Hromada, and A. D. Cronin, Phys. Rev. Lett. **109**, 243004 (2012).

[27] A. Derevianko, Phys. Rev. Lett. **85**, 1618 (2000).

[28] B. K. Sahoo, R. Chaudhuri, B. P. Das, and D. Mukherjee, Phys. Rev. Lett. **96**, 163003 (2006).

[29] S. G. Porsev, K. Beloy, and A. Derevianko, Phys. Rev. Lett. **102**, 181601 (2009).

[30] R. H. Leonard, A. J. Fallon, C. A. Sackett, and M. S. Safronova, Phys. Rev. A **92**, 052501 (2015).

[31] M. Enderlein, T. Huber, C. Schneider, and T. Schaetz, Phys. Rev. Lett. **109**, 233004 (2012).

[32] I. Krasnov and L. Kamenshchikov, Opt. Commun. **312**, 192 (2014).

[33] Y. Huang, J. Cao, P. Liu, K. Liang, B. Ou, H. Guan, X. Huang, T. Li, and K. Gao, Phys. Rev. A **85**, 030503(R) (2012).

[34] C. Degenhardt, H. Stoehr, U. Sterr, F. Riehle, and C. Lisdat, Phys. Rev. A **70**, 023414 (2004).

[35] M. Chwalla, J. Benhelm, K. Kim, G. Kirchmair, T. Monz, M. Riebe, P. Schindler, A. S. Villar, W. Hänsel, C. F. Roos *et al.*, Phys. Rev. Lett. **102**, 023002 (2009).

[36] P. Zhang, J. Cao, H.-L. Shu, J.-b. Yuan, J.-J. Shang, K.-f. Cui, S.-j. Chao, S.-m. Wang, D.-x. Liu, and X.-r. Huang, J. Phys. B **50**, 015002 (2017).

[37] H. Hffner, C. Roos, and R. Blatt, Phys. Rep. **469**, 155 (2008).

[38] J. Kaur, S. Singh, B. Arora, and B. K. Sahoo, Phys. Rev. A **95**, 042501 (2017).

[39] J. Jiang, J. Mitroy, Y. Cheng, and M. W. J. Bromley, Phys. Rev. A **94**, 062514 (2016).

[40] I. P. Grant and H. M. Quiney, Phys. Rev. A **62**, 022508 (2000).

[41] I. P. Grant, *Relativistic Quantum Theory of Atoms and Molecules: Theory and Computation* (Springer, New York, 2007).

[42] S. Kaneko, J. Phys. B **10**, 3347 (1977).

[43] W. Müller, J. Flesch, and W. Meyer, J. Chem. Phys. **80**, 3297 (1984).

[44] M. S. Safronova and U. I. Safronova, Phys. Rev. A **83**, 012503 (2011).

[45] See Supplemental Material at http://link.aps.org/supplemental/10.1103/PhysRevA.96.042503 for additional tables of energy levels and matrix elements and breakdowns of polarizabilities at the magic wavelengths.

[46] N. L. Manakov, V. D. Ovsiannikov, and L. P. Rapoport, Phys. Rep. **141**, 320 (1986).

[47] K. Beloy, Ph.D. thesis, University of Nevada, 2009.

[48] B. K. Sahoo, B. P. Das, and D. Mukherjee, Phys. Rev. A **79**, 052511 (2009).